








**Atomic photoexcitation as a tool for probing purity of twisted light modes**R. P. Schmidt <sup>1,2,\*</sup> S. Ramakrishna <sup>3,4,5</sup> A. A. Peshkov <sup>1,2</sup> N. Huntemann <sup>1</sup> E. Peik <sup>1</sup>  
S. Fritzsche <sup>3,4,5</sup> and A. Surzhykov <sup>1,2,6</sup><sup>1</sup>Physikalisch-Technische Bundesanstalt, Bundesallee 100, D-38116 Braunschweig, Germany<sup>2</sup>Institut für Mathematische Physik, Technische Universität Braunschweig, Mendelssohnstrasse 3, D-38106 Braunschweig, Germany<sup>3</sup>Helmholtz-Institut Jena, Fröbelstieg 3, D-07763 Jena, Germany<sup>4</sup>GSI Helmholtzzentrum für Schwerionenforschung GmbH, Planckstrasse 1, D-64291 Darmstadt, Germany<sup>5</sup>Theoretisch-Physikalisches Institut, Friedrich-Schiller-Universität Jena, D-07763 Jena, Germany<sup>6</sup>Laboratory for Emerging Nanometrology Braunschweig, Langer Kamp 6a/b, D-38106 Braunschweig, Germany

(Received 13 October 2023; accepted 26 January 2024; published 4 March 2024)

The twisted light modes used in modern atomic physics experiments can be contaminated by small admixtures of plane-wave radiation. Although these admixtures hardly reveal themselves in the beam-intensity profile, they may seriously affect the outcome of high-precision spectroscopy measurements. In the present study we propose a method for diagnosing such a plane-wave contamination which is based on the analysis of the magnetic sublevel population of atoms or ions interacting with the “twisted + plane-wave” radiation. In order to theoretically investigate the sublevel populations, we solve the Liouville–von Neumann equation for the time evolution of the atomic density matrix. The proposed method is illustrated for the electric dipole  $5s\ ^2S_{1/2} - 5p\ ^2P_{3/2}$  transition in Rb induced by (linearly, radially, or azimuthally polarized) vortex light with just a small contamination. We find that even tiny admixtures of plane-wave radiation can lead to remarkable variations in the populations of the ground-state magnetic sublevels. This opens up new opportunities for diagnostics of twisted light in atomic spectroscopy experiments.

DOI: [10.1103/PhysRevA.109.033103](https://doi.org/10.1103/PhysRevA.109.033103)**I. INTRODUCTION**

For more than 30 years, twisted light has attracted considerable interest in many areas of modern physics. In contrast to conventional plane waves, such beams exhibit a highly inhomogeneous intensity profile, a complex polarization texture, and a phase singularity [1–3]. Twisted beams have found application in optical traps [4,5] and tweezers [6,7], classical and quantum communication [8,9], superresolution optical sensing [10,11] and imaging [12,13], and atomic magnetometers [14,15]. Moreover, they were recently used for high-precision spectroscopy of trapped ions. In particular, Laguerre-Gaussian (LG) beams were employed to coherently excite clock transitions in single  $\text{Ca}^+$  [16] and  $\text{Yb}^+$  ions [17]. The interpretation of such experiments, however, can be complicated by incomplete knowledge of the radiation composition. For the analysis of the  $\text{Ca}^+$  experiment, for instance, Afanasev *et al.* [18] inferred that the light initially assumed to be circularly polarized was slightly elliptically polarized. Furthermore, a radially polarized beam produced by a vortex retarder was suspected to be contaminated by a small amount of plane-wave admixture in the  $\text{Yb}^+$  experiment of Lange *et al.* [17]. Such impurity of incident light is one of the major challenges to tackle in high-precision spectroscopy experiments with twisted radiation.

A conventional method to obtain information about the mode composition of radiation is to analyze its intensity

profile. This approach has a natural limitation in the domain of relatively small admixtures to the leading mode since they do not cause noticeable changes in intensity distribution. Although tiny impurities are “invisible” for the conventional method, they may significantly affect the population dynamics of a target atom, which is usually observed in the form of Rabi oscillations. In this contribution, we discuss the effect of admixture of plane-wave radiation to the leading twisted mode and propose an approach to investigate this admixture, which shows its full potential in the case of tiny impurities. Our approach is based on an analysis of the populations of the ground-state magnetic sublevels of an atom interacting with laser radiation. These populations can be measured, for example, by state-dependent fluorescence [16,19].

The present work is organized as follows. In Sec. II A we briefly recall the basic formulas needed to describe the incident radiation and define the geometry for the light-atom coupling. This coupling is described by transition-matrix elements whose evaluation is discussed in Sec. II B. In order to analyze the time evolution of atomic populations, in Sec. II C we lay down the density-matrix formalism based on the Liouville–von Neumann equation. Substituting the transition-matrix elements into the Liouville–von Neumann equation, we compute elements of the density matrix at each instant of time. For analysis and guidance of experimental studies, however, it is more convenient to describe the system in terms of the so-called statistical tensors. These tensors are related to the population of atomic sublevels and characterize the orientation of the system, as shown in Sec. II D. The general theory is

\*riaan.schmidt@ptb.de

applied to the specific case of the  $5s^2S_{1/2} - 5p^2P_{3/2}$  transition in Rb induced by a Bessel beam with a small admixture of a plane wave. The calculations presented in Sec. III indicate that even tiny admixtures can significantly affect the population of the  $M_g = \pm 1/2$  ground-state sublevels. Moreover, we show how the impurity effects can be controlled by applying an external magnetic field. Finally, a summary of our results and an outlook are given in Sec. IV.

## II. THEORY

### A. Twisted light modes

Modern experiments on the interaction of trapped atoms or ions with twisted radiation usually employ LG modes. Theoretical analysis of the coupling between these modes and atoms is a rather complicated task which can be simplified by approximating LG radiation with a Bessel beam. Such an approximation is well justified when an atom is located in the vicinity of the beam center [17,20]. Similarly, the radiation in the center of a Gaussian LG<sub>00</sub> mode can be approximated by a plane wave when the spatial mode extent is large compared to the atomic sample. The vector potentials for both Bessel and plane waves will be introduced below.

#### 1. Photon vector potential

Since the interaction of atoms with twisted and plane-wave radiation has already been widely discussed in the literature [21–27], we present here only a few basic formulas needed for our theoretical analysis. We start with the vector potential for a plane wave, which may be written in the Coulomb gauge as

$$\mathbf{A}_\lambda^{(\text{pl})}(\mathbf{r}) = A_0 \mathbf{e}_{k\lambda} e^{i\mathbf{k}\cdot\mathbf{r}}, \quad (1)$$

where  $\mathbf{k}$  and  $\mathbf{e}_{k\lambda}$  are the photon wave and polarization vectors,  $\omega = kc$  is its frequency,  $\lambda = \pm 1$  denotes the helicity, and  $A_0$  is the amplitude, which will be specified later. A Bessel beam is, in turn, characterized by the vector potential

$$\mathbf{A}_{m_\gamma, \lambda}^{(\text{tw})}(\mathbf{r}) = A_0 \int a_{\varkappa m_\gamma}(\mathbf{k}_\perp) \mathbf{e}_{k\lambda} e^{i\mathbf{k}\cdot\mathbf{r}} \frac{d^2\mathbf{k}_\perp}{(2\pi)^2}, \quad (2)$$

with the weight function

$$a_{\varkappa m_\gamma}(\mathbf{k}_\perp) = \frac{2\pi}{\varkappa} (-i)^{m_\gamma} e^{im_\gamma\phi_k} \delta(k_\perp - \varkappa). \quad (3)$$

The latter vector potential describes a beam with amplitude  $A_0$ , helicity  $\lambda$ , longitudinal ( $k_z$ ) and transverse ( $\varkappa$ ) components of the linear momentum, and projection  $m_\gamma$  of the total angular momentum onto the light propagation direction [28,29]. It follows from Eqs. (1)–(3) that the Bessel beam can be seen as a coherent superposition of plane waves whose wave vectors  $\mathbf{k}$  are uniformly distributed upon the surface of a cone with a polar opening angle  $\theta_k = \arctan(\varkappa/k_z)$ .

In Eqs. (1)–(3), we introduced helicity states which are related to circularly polarized light. The other polarizations can readily be constructed from these helicity states. For example, plane waves that are linearly polarized parallel or

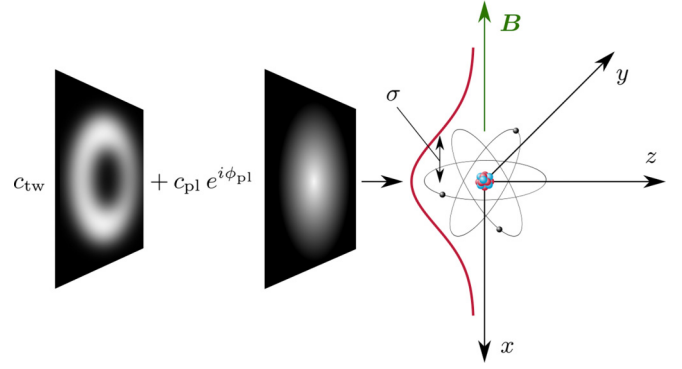


FIG. 1. Geometry of the excitation of a single atom by a superposition (9) of Bessel and plane waves. The quantization axis is chosen along the applied magnetic field, which is perpendicular to the light propagation direction. The atom is either perfectly localized in the beam center or delocalized with distribution width  $\sigma$ .

perpendicular to a reaction plane [30], defined by the direction of light propagation and an external magnetic field  $\mathbf{B}$ , are

$$\mathbf{A}_x^{(\text{pl})} = \frac{1}{\sqrt{2}} [\mathbf{A}_{\lambda=-1}^{(\text{pl})} + \mathbf{A}_{\lambda=+1}^{(\text{pl})}], \quad (4a)$$

$$\mathbf{A}_y^{(\text{pl})} = \frac{i}{\sqrt{2}} [\mathbf{A}_{\lambda=-1}^{(\text{pl})} - \mathbf{A}_{\lambda=+1}^{(\text{pl})}]; \quad (4b)$$

see Fig. 1 for further details. In a similar way, one can also construct linearly polarized twisted modes,

$$\mathbf{A}_x^{(\text{tw})} = \frac{i}{\sqrt{2}} [\mathbf{A}_{m_{\gamma_1}, \lambda=+1}^{(\text{tw})} - \mathbf{A}_{m_{\gamma_2}, \lambda=-1}^{(\text{tw})}], \quad (5a)$$

$$\mathbf{A}_y^{(\text{tw})} = \frac{1}{\sqrt{2}} [\mathbf{A}_{m_{\gamma_1}, \lambda=+1}^{(\text{tw})} + \mathbf{A}_{m_{\gamma_2}, \lambda=-1}^{(\text{tw})}], \quad (5b)$$

where  $m_{\gamma_1} - m_{\gamma_2} = 2$ , as discussed in Ref. [29]. Furthermore, in contrast to plane waves, twisted radiation provides a richer choice of polarization patterns. For instance, the radially and azimuthally polarized beams read

$$\mathbf{A}_{\text{rad}}^{(\text{tw})} = -\frac{i}{\sqrt{2}} [\mathbf{A}_{m_\gamma=0, \lambda=+1}^{(\text{tw})} + \mathbf{A}_{m_\gamma=0, \lambda=-1}^{(\text{tw})}], \quad (6a)$$

$$\mathbf{A}_{\text{az}}^{(\text{tw})} = -\frac{1}{\sqrt{2}} [\mathbf{A}_{m_\gamma=0, \lambda=+1}^{(\text{tw})} - \mathbf{A}_{m_\gamma=0, \lambda=-1}^{(\text{tw})}]. \quad (6b)$$

It can easily be seen that the vector potentials (5) and (6) correspond to linear, radial, and azimuthal polarizations in the paraxial regime where the opening angle  $\theta_k$  is small. In this regime the spin and orbital angular momenta are decoupled from each other, and Eq. (2) is simplified to

$$\mathbf{A}_{m_\gamma, \lambda}^{(\text{tw})}(\mathbf{r}) \approx \mathbf{A}_{m_l, \lambda}^{(\text{par})}(\mathbf{r}) = \mathbf{e}_\lambda (-i)^\lambda J_{m_l}(\varkappa r_\perp) e^{im_l\phi} e^{ik_z z}, \quad (7)$$

where  $m_l = m_\gamma - \lambda$  is the projection of the orbital angular momentum,  $\mathbf{e}_\lambda = \mathbf{e}_{\mathbf{k}\parallel z, \lambda}$  is the polarization vector,  $J_{m_l}(\varkappa r_\perp)$  stands for the Bessel function, and  $r_\perp$ ,  $\phi$ , and  $z$  are cylindrical coordinates [28]. By using Eqs. (5)–(7), we obtain

$$\mathbf{A}_x^{(\text{par})} = \mathbf{e}_x J_{m_l}(\varkappa r_\perp) e^{im_l\phi} e^{ik_z z}, \quad (8a)$$

$$\mathbf{A}_y^{(\text{par})} = \mathbf{e}_y J_{m_l}(\varkappa r_\perp) e^{im_l\phi} e^{ik_z z}, \quad (8b)$$

$$\mathbf{A}_{\text{rad}}^{(\text{par})} = \mathbf{e}_r J_1(\varkappa r_\perp) e^{ik_z z}, \quad (8c)$$

$$\mathbf{A}_{\text{az}}^{(\text{par})} = \mathbf{e}_\phi J_1(\varkappa r_\perp) e^{ik_z z}, \quad (8d)$$

where  $\mathbf{e}_x$ ,  $\mathbf{e}_y$ ,  $\mathbf{e}_r$ , and  $\mathbf{e}_\phi$  are the basis unit vectors in Cartesian and cylindrical coordinates, respectively. Strictly speaking, solutions (8c) and (8d) do not possess a well-defined orbital angular momentum projection and therefore cannot be referred to as twisted light. Usually, such fields are called vector beams [15,31].

## 2. Superposition of two modes

As already mentioned above, incident radiation may not always be produced in a pure twisted state. Instead, a target atom can be exposed to a superposition of different modes which contains the LG<sub>00</sub> one as well. In order to model the impact of such an admixture, we will add a plane-wave component to the twisted light,

$$\mathbf{A}^{(\text{mix})} = c_{\text{tw}}\mathbf{A}^{(\text{tw})} + c_{\text{pl}} e^{i\phi_{\text{pl}}}\mathbf{A}^{(\text{pl})}, \quad (9)$$

where the real mixture coefficients  $c_{\text{tw}}$  and  $c_{\text{pl}}$  satisfy the normalization condition  $c_{\text{tw}}^2 + c_{\text{pl}}^2 = 1$  and  $\phi_{\text{pl}}$  is the relative phase of the two light modes. In general, this relative phase can affect not only the beam-intensity profile but also its polarization texture.

Below we will discuss a method for determining the weight  $c_{\text{pl}}$  and phase  $\phi_{\text{pl}}$  of the plane-wave component based on the analysis of the population dynamics of magnetic sublevels in a target atom exposed to the radiation (9). This requires a choice of the quantization axis of the overall system. In our study we will utilize geometry similar to what is used in Hanle-effect

experiments [32–36]; i.e., the atomic quantization axis is chosen to be along the magnetic field applied perpendicular to the light propagation direction (see Fig. 1).

## B. Evaluation of the transition-matrix element

Having discussed the vector potentials of Bessel and plane waves, we are ready now to examine their interaction with an atom. In particular, we will question the laser-induced transition between ground  $|\alpha_g J_g M_g\rangle$  and excited  $|\alpha_e J_e M_e\rangle$  atomic states whose properties can be traced back to the first-order matrix element

$$V_{eg} = ec \langle \alpha_e J_e M_e | \sum_q \boldsymbol{\alpha}_q \cdot \mathbf{A}(\mathbf{r}_q) | \alpha_g J_g M_g \rangle, \quad (10)$$

where  $J$  denotes the total angular momentum,  $M$  is its projection on the atomic quantization axis, and  $\alpha$  refers to all additional quantum numbers. Moreover,  $q$  runs over all electrons in a target atom, and  $\boldsymbol{\alpha}_q$  denotes the vector of Dirac matrices for the  $q$ th particle [37]. This matrix element depends on a particular choice of the vector potential  $\mathbf{A}$ . For the superposition of twisted and plane-wave radiation (9), we have

$$V_{eg}^{(\text{mix})} = c_{\text{tw}} V_{eg}^{(\text{tw})} + c_{\text{pl}} e^{i\phi_{\text{pl}}} V_{eg}^{(\text{pl})}. \quad (11)$$

The evaluation of the twisted ( $V_{eg}^{(\text{tw})}$ ) and plane-wave ( $V_{eg}^{(\text{pl})}$ ) matrix elements has already been discussed in detail in the literature [29,38]. For the geometry shown in Fig. 1, where light propagates along the  $z$  axis perpendicular to the atomic quantization axis, they read

$$V_{eg}^{(\text{pl})}(\lambda) = A_0 ec \sqrt{2\pi} i^L (i\lambda)^p \frac{[L]^{1/2}}{[J_e]^{1/2}} d_{M_e - M_g, \lambda}^L(\pi/2) \langle J_g M_g L M_e - M_g | J_e M_e \rangle \langle \alpha_e J_e | H_\gamma(pL) | \alpha_g J_g \rangle, \quad (12)$$

$$V_{eg}^{(\text{tw})}(\lambda) = A_0 ec \sqrt{2\pi} \sum_M i^{L+M} (i\lambda)^p (-1)^{m_\gamma} \frac{[L]^{1/2}}{[J_e]^{1/2}} e^{i(m_\gamma - M)\phi_b} J_{m_\gamma - M}(\lambda b) d_{M, \lambda}^L(\theta_k) d_{M_e - M_g, M}^L(\pi/2) \times \langle J_g M_g L M_e - M_g | J_e M_e \rangle \langle \alpha_e J_e | H_\gamma(pL) | \alpha_g J_g \rangle, \quad (13)$$

where we have assumed, moreover, that both light-field components are circularly polarized. Here, the reduced matrix element  $\langle \alpha_e J_e | H_\gamma(pL) | \alpha_g J_g \rangle$  for a magnetic ( $p=0$ ) or electric ( $p=1$ ) transition of multipolarity  $L$  depends on the electronic structure of an atom, and its evaluation will be discussed later. Furthermore, in Eqs. (12) and (13)  $d_{M, \lambda}^L(\theta_k)$  is the small Wigner  $D$  function, and  $[J] = 2J + 1$ .

We note that the matrix element (13) also depends on the impact parameter  $\mathbf{b} = (b \cos \phi_b, b \sin \phi_b, 0)$ , which specifies the position of a target atom with respect to the beam center. The introduction of this parameter is necessary since the Bessel beam exhibits an inhomogeneous intensity profile with a central dark spot at  $b=0$  [31]. In contrast to Bessel beams, the intensity and phase of plane waves do not depend on spatial position, and hence, there is no need to add  $\mathbf{b}$  to Eq. (12).

Similar to the discussion in Sec. II A 1, the matrix elements (12) and (13) can be used as *building blocks* to investigate cases of polarization different from circular. For example,

in order to analyze the interaction of an atom with linearly polarized plane or twisted waves, one should use

$$V_{eg}^{(\text{pl})}(x) = \frac{1}{\sqrt{2}} [V_{eg}^{(\text{pl})}(\lambda = -1) + V_{eg}^{(\text{pl})}(\lambda = +1)], \quad (14a)$$

$$V_{eg}^{(\text{pl})}(y) = \frac{i}{\sqrt{2}} [V_{eg}^{(\text{pl})}(\lambda = -1) - V_{eg}^{(\text{pl})}(\lambda = +1)], \quad (14b)$$

$$V_{eg}^{(\text{tw})}(x) = \frac{i}{\sqrt{2}} [V_{eg}^{(\text{tw})}(\lambda = +1) - V_{eg}^{(\text{tw})}(\lambda = -1)], \quad (14c)$$

$$V_{eg}^{(\text{tw})}(y) = \frac{1}{\sqrt{2}} [V_{eg}^{(\text{tw})}(\lambda = +1) + V_{eg}^{(\text{tw})}(\lambda = -1)]. \quad (14d)$$

In a similar way one can construct matrix elements for the interaction with radially or azimuthally polarized vector beams.

## C. Density-matrix formalism

Due to the interaction of atoms with light, the populations of atomic ground and excited states can vary with time. To

investigate the time dependence of atomic-level populations, it is practical to use the time-dependent density-matrix theory [39], where a state of the system is represented by the density operator  $\hat{\rho}(t)$  satisfying the Liouville–von Neumann equation:

$$\frac{d}{dt}\hat{\rho}(t) = -\frac{i}{\hbar}[\hat{H}(t), \hat{\rho}(t)] + \hat{R}(t). \quad (15)$$

Here,  $\hat{H}(t)$  is the total Hamiltonian of an atom in the presence of both the magnetic field and the incident radiation. Moreover, the operator  $\hat{R}(t)$  has been introduced to take into account phenomenologically the relaxation processes; see Refs. [40,41] for more details.

In order to express the operator  $\hat{\rho}(t)$  in matrix form, a convenient set of basis states must be chosen. In our work we use the ground ( $|\alpha_g J_g M_g\rangle$ ) and excited ( $|\alpha_e J_e M_e\rangle$ ) atomic

states as a basis. In this basis, the matrix elements of  $\hat{\rho}(t)$ , also known as the density matrix, take the form

$$\rho_{gg'}(t) = \langle \alpha_g J_g M_g | \hat{\rho}(t) | \alpha_g J_g M_g' \rangle, \quad (16a)$$

$$\rho_{ee'}(t) = \langle \alpha_e J_e M_e | \hat{\rho}(t) | \alpha_e J_e M_e' \rangle, \quad (16b)$$

$$\rho_{ge}(t) = \langle \alpha_g J_g M_g | \hat{\rho}(t) | \alpha_e J_e M_e \rangle, \quad (16c)$$

$$\rho_{eg}(t) = \langle \alpha_e J_e M_e | \hat{\rho}(t) | \alpha_g J_g M_g \rangle. \quad (16d)$$

Here, the notations  $\rho_{gg}(t)$  and  $\rho_{ee}(t)$  are used as shorthand for the probability of finding an atom in substates  $|\alpha_g J_g M_g\rangle$  and  $|\alpha_e J_e M_e\rangle$ , respectively, while  $\rho_{gg'}(t)$  and  $\rho_{ee'}(t)$  describe the coherences between different substates [42]. In the present work we focus especially on the ground-state density matrix and investigate its dependence on the magnetic-field strength for different compositions of incident radiation.

From Eqs. (15) and (16), we obtain the following set of differential equations for the density-matrix elements:

$$\frac{d}{dt}\tilde{\rho}_{gg'}(t) = -i\Omega_g^{(L)}(M_g - M_g')\tilde{\rho}_{gg'}(t) - \frac{i}{2\hbar}\left[\sum_{\tilde{M}_e} V_{e\tilde{g}}^* \tilde{\rho}_{e\tilde{g}'}(t) - \sum_{\tilde{M}_e} V_{\tilde{e}g} \tilde{\rho}_{\tilde{e}g}(t)\right] + R_{gg'}(t), \quad (17a)$$

$$\frac{d}{dt}\tilde{\rho}_{ee'}(t) = -i\Omega_e^{(L)}(M_e - M_e')\tilde{\rho}_{ee'}(t) - \frac{i}{2\hbar}\left[\sum_{\tilde{M}_g} V_{e\tilde{g}} \tilde{\rho}_{\tilde{g}e'}(t) - \sum_{\tilde{M}_g} V_{e'\tilde{g}}^* \tilde{\rho}_{e'\tilde{g}}(t)\right] + R_{ee'}(t), \quad (17b)$$

$$\frac{d}{dt}\tilde{\rho}_{ge}(t) = -i\Delta\tilde{\rho}_{ge}(t) + i(\Omega_e^{(L)}M_e - \Omega_g^{(L)}M_g)\tilde{\rho}_{ge}(t) - \frac{i}{2\hbar}\left[\sum_{\tilde{M}_e} V_{e\tilde{g}}^* \tilde{\rho}_{\tilde{e}e}(t) - \sum_{\tilde{M}_g} V_{e\tilde{g}}^* \tilde{\rho}_{\tilde{g}g}(t)\right] + R_{ge}(t), \quad (17c)$$

$$\frac{d}{dt}\tilde{\rho}_{eg}(t) = i\Delta\tilde{\rho}_{eg}(t) - i(\Omega_e^{(L)}M_e - \Omega_g^{(L)}M_g)\tilde{\rho}_{eg}(t) - \frac{i}{2\hbar}\left[\sum_{\tilde{M}_g} V_{e\tilde{g}} \tilde{\rho}_{\tilde{g}g}(t) - \sum_{\tilde{M}_e} V_{\tilde{e}g} \tilde{\rho}_{\tilde{e}e}(t)\right] + R_{eg}(t). \quad (17d)$$

Here, we have made the substitutions

$$\tilde{\rho}_{gg'}(t) = \rho_{gg'}(t), \quad (18a)$$

$$\tilde{\rho}_{ee'}(t) = \rho_{ee'}(t), \quad (18b)$$

$$\tilde{\rho}_{ge}(t) = \rho_{ge}(t)e^{-i\omega t}, \quad (18c)$$

$$\tilde{\rho}_{eg}(t) = \rho_{eg}(t)e^{i\omega t} \quad (18d)$$

and employed the rotating-wave approximation, which consists of neglecting the fast-oscillating terms proportional to  $e^{\pm 2i\omega t}$  [43,44]. Furthermore,  $\Omega^{(L)} = g_J \mu_B B / \hbar$  is the Larmor frequency, and  $\Delta = \omega - \omega_0$  is the frequency detuning of the radiation from the atomic resonance at  $\omega_0$ .

In Eqs. (17), the terms  $R(t)$  account phenomenologically for the relaxation of an atom due to spontaneous emission. To derive these terms, we follow the procedure discussed in Refs. [39,45] and find

$$R_{gg'}(t) = \Gamma \sum_{M_e, M_e', M} \langle J_g M_g L M | J_e M_e \rangle \tilde{\rho}_{ee'}(t) \times \langle J_g M_g' L M | J_e M_e' \rangle, \quad (19a)$$

$$R_{ee'}(t) = -\Gamma \tilde{\rho}_{ee'}(t), \quad (19b)$$

$$R_{ge}(t) = -\frac{\Gamma}{2} \tilde{\rho}_{ge}(t), \quad (19c)$$

$$R_{eg}(t) = -\frac{\Gamma}{2} \tilde{\rho}_{eg}(t), \quad (19d)$$

with  $\Gamma$  being the decay rate of the excited state. In obtaining Eqs. (19), we have assumed that only one dominant channel with multipolarity  $L$  contributes to the decay.

#### D. Statistical tensors of atomic states

Solving Eqs. (17) numerically, we find the atomic density matrix at each particular moment in time. In order to visualize the results and simplify the discussion, it is more convenient to describe the population of atomic sublevels in terms of the statistical tensors [46] that are linear combinations of the density-matrix elements,

$$\rho_{kq}(\alpha J; t) = \sum_{M M'} (-1)^{J-M'} \langle J M J - M' | k q \rangle \times \langle \alpha J M | \hat{\rho}(t) | \alpha J M' \rangle. \quad (20)$$

These tensors have well-defined symmetry properties since they transform like spherical harmonics of rank  $k$  under a rotation of the coordinates. In atomic physics,  $\rho_{kq}$  are usually normalized as

$$A_{kq}(\alpha J; t) = \frac{\rho_{kq}(\alpha J; t)}{\rho_{00}(\alpha J; t)} \quad (21)$$

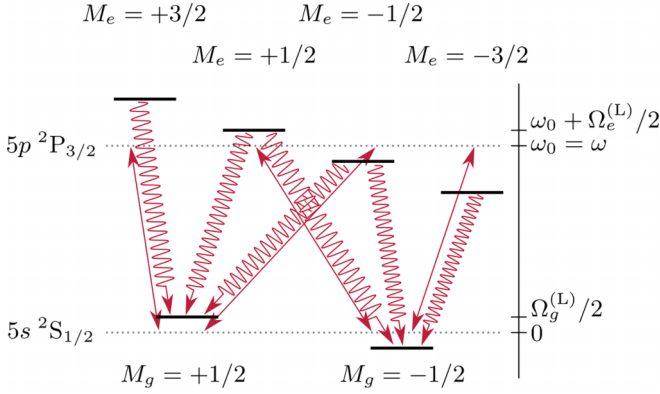


FIG. 2. The transition scheme for the  $5s\ ^2S_{1/2}$ - $5p\ ^2P_{3/2}$  excitation of rubidium, along with the Zeeman splitting of the magnetic sublevels. The arrows represent the transition as induced by  $y$ -polarized incident light (9) with  $m_l = +1$ , and the wavy lines represent spontaneous decay.

to produce the so-called alignment and orientation parameters. These parameters characterize the relative population of magnetic sublevels  $|\alpha JM\rangle$  and coherence between them. If all magnetic sublevels are equally populated, the atom is unpolarized, and the only nonzero parameter is  $\mathcal{A}_{00} = 1$ . In contrast, unequal substate populations lead to at least one nonvanishing parameter  $\mathcal{A}_{kq}$  with  $k > 0$ . If the system is characterized by parameters  $\mathcal{A}_{kq}$  of even rank  $k$ , it is said to be aligned, while the system is called oriented if at least one odd-rank parameter  $\mathcal{A}_{kq}$  is nonzero [46].

In what follows we investigate the population of the  $5s\ ^2S_{1/2}$  state, which can be described by only three nontrivial parameters  $\mathcal{A}_{1q}$ , with  $q = 0, \pm 1$ . Here,  $\mathcal{A}_{10}$  describes the difference in the population of magnetic sublevels,

$$\mathcal{A}_{10}(t) = \frac{\rho_{+1/2}(t) - \rho_{-1/2}(t)}{\rho_{+1/2}(t) + \rho_{-1/2}(t)}, \quad (22)$$

with

$$\rho_{M_g}(t) = \langle 5s\ ^2S_{1/2}\ M_g | \hat{\rho}(t) | 5s\ ^2S_{1/2}\ M_g \rangle, \quad (23)$$

and hence characterizes the orientation of the  $5s\ ^2S_{1/2}$  state, while parameters  $\mathcal{A}_{1\pm 1}$  reflect coherences between different substates.

In the next section, we analyze the dependence of the orientation parameters  $\mathcal{A}_{1q}$  on the external magnetic-field strength for different mixtures of incident radiation to determine the weight and phase of the plane-wave admixture.

### III. RESULTS AND DISCUSSION

In the previous section we derived the Liouville–von Neumann equation (17), which allows us to investigate the time-dependent interaction of an atom with a beam propagating along the  $z$  axis in the presence of a magnetic field ( $\mathbf{B} \perp \mathbf{e}_z$ ). Below we will use this theory to explore the interaction of Rb atom, initially prepared in the unpolarized  $5s\ ^2S_{1/2}$  state, with the superposition (9) of twisted and plane waves. Both modes are supposed to drive the  $5s\ ^2S_{1/2}$ - $5p\ ^2P_{3/2}$  electric dipole ( $E1$ ) transition of frequency  $\omega_0 = 2\pi \times 384$  THz (see Fig. 2).

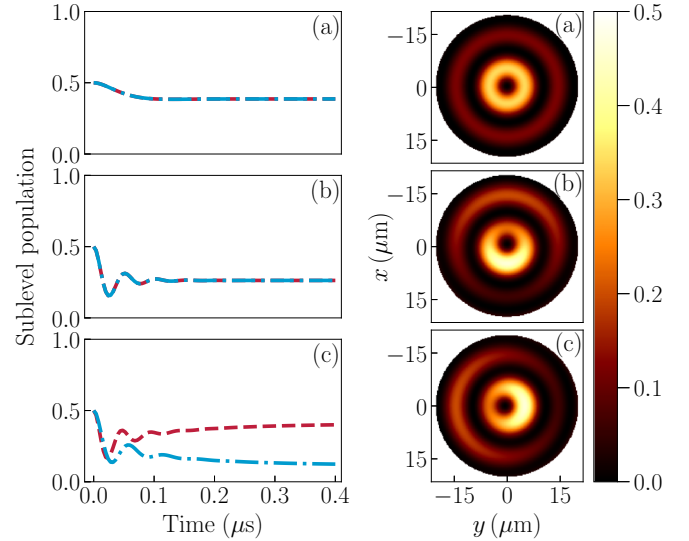


FIG. 3. Left: Populations of the  $M_g = -1/2$  (dashed line) and  $M_g = +1/2$  (dash-dotted line) magnetic sublevels of the  $5s\ ^2S_{1/2}$  ground state of rubidium well localized on the vortex line,  $b = 0$ , as a function of time for zero magnetic field,  $B = 0$ . The incident light (9) is assumed to be a superposition of  $y$ -polarized plane and Bessel waves, where the latter carries the orbital angular momentum projection  $m_l = +1$  and has the opening angle  $\theta_k = 2.49^\circ$ . Results are presented for (a) the pure Bessel beam,  $c_{\text{pl}} = 0$ , and superpositions with (b)  $c_{\text{pl}} = 0.1$  and  $\phi_{\text{pl}} = 0^\circ$  and (c)  $c_{\text{pl}} = 0.1$  and  $\phi_{\text{pl}} = 90^\circ$ . Right: Transverse intensity profiles of these beams in units of  $A_0^2$ .

The numerical solution of Eqs. (17) requires further information about the incident radiation and the target atom. In particular, we need to know the spontaneous decay rate  $\Gamma$  and the reduced matrix element  $\langle 5p\ ^2P_{3/2} || H_\gamma(E1) || 5s\ ^2S_{1/2} \rangle$  which enter into Eqs. (11)–(13) and (19). Their values were obtained using the package JAC, which was developed to calculate energies and transition probabilities in many-electron atoms [47]. Moreover, the light amplitude  $A_0 = 2.54 \times 10^{-12}$  and the opening angle  $\theta_k = 2.49^\circ$  are chosen so that the plane (1) and twisted (2) waves reproduce the LG<sub>00</sub> and LG<sub>01</sub> modes with a total power of  $4\ \mu\text{W}$  and a waist of  $7\ \mu\text{m}$  in the vicinity of the beam center. Finally, we assume that the detuning of the light from the atomic resonance in the absence of a magnetic field is zero,  $\Delta = 0$ .

#### A. Localized atom in the absence of magnetic field

As seen from Eq. (13), we have to agree on the value of the impact parameter  $b$  to find a solution of the Liouville–von Neumann equation (17). In this section, we consider an idealized scenario in which the atom is well localized on the vortex line at  $b = 0$ . For this scenario, the left column of Fig. 3 displays the time evolution of the populations  $\rho_{-1/2}(t)$  and  $\rho_{+1/2}(t)$  of the ground-state magnetic sublevels  $M_g = \pm 1/2$ . The calculations were made in the limit of vanishing magnetic field,  $B = 0$ , for different superpositions (9) of twisted and plane waves. Moreover, we assumed that both components of light,  $\mathbf{A}^{(\text{tw})}$  with  $m_l = +1$  and  $\mathbf{A}^{(\text{pl})}$ , are linearly polarized along the  $y$  axis (see Fig. 1). As illustrated in Fig. 3, the population dynamics is very sensitive to the composition of

incident light. For example, if the atom interacts with pure Bessel radiation,  $c_{\text{pl}} = 0$ , both  $M_g = \pm 1/2$  sublevels are always equally populated,  $\rho_{-1/2}(t) = \rho_{+1/2}(t)$ . This resembles the outcome of photoexcitation by linearly polarized plane waves which is known to produce no orientation of the target along an axis normal to both light propagation and polarization directions. A similar result is obtained for the superposition of twisted and plane waves with relative phase  $\phi_{\text{pl}} = 0^\circ$  [see the left panel of Fig. 3(b)]. In contrast, qualitatively different behavior can be observed when the Bessel- and plane-wave components are phase shifted with respect to each other. This effect is most pronounced for the case  $\phi_{\text{pl}} = 90^\circ$ , which is displayed in Fig. 3(c). As seen from Fig. 3(c), the populations of the  $M_g = \pm 1/2$  sublevels gradually diverge from each other as time progresses and reach the values  $\rho_{-1/2} = 0.40$  and  $\rho_{+1/2} = 0.12$  for the steady state. This result clearly indicates that the admixture of a plane wave to a Bessel wave can lead to significant orientation of the  $5s^2S_{1/2}$  ground state, even though both components of the beam are linearly polarized.

To explain the qualitatively different behavior of the sublevel populations  $\rho_{\pm 1/2}(t)$ , in the right column of Fig. 3 we compare three different transverse intensity profiles of the incident beams. As seen from Fig. 3(a), the intensity profile of a pure Bessel beam has the well-known annular structure which is axially symmetric with respect to the vortex line crossing the transverse plane at  $x = y = 0$ . This symmetry is broken by an admixture of plane-wave radiation. The symmetry breaking can easily be understood if we consider the absolute value squared of the vector potential describing the y-polarized superposition:

$$\begin{aligned} |\mathbf{A}^{(\text{mix})}(r, \phi, z = 0)|^2 & \simeq |\mathbf{A}^{(\text{tw})}(r)e^{im_l\phi} + \mathbf{A}^{(\text{pl})}(r)e^{i\phi_{\text{pl}}}|^2 \\ & = |\mathbf{A}^{(\text{tw})}(r)|^2 + |\mathbf{A}^{(\text{pl})}(r)|^2 \\ & \quad + 2\mathbf{A}^{(\text{tw})}(r)\mathbf{A}^{(\text{pl})}(r)\cos(m_l\phi - \phi_{\text{pl}}). \end{aligned} \quad (24)$$

As seen from this equation, the interference term containing  $\cos(m_l\phi - \phi_{\text{pl}})$  depends on the azimuthal angle  $\phi$  and hence violates the axial symmetry of the beam. In addition, the resulting asymmetric intensity profile of the ‘‘Bessel-wave + plane-wave’’ mixture depends on the relative phase  $\phi_{\text{pl}}$ . For  $\phi_{\text{pl}} = 0^\circ$ , the incident beam is symmetric with respect to the  $x$ - $z$  plane containing the quantization axis and the light propagation direction, while this is not the case when  $\phi_{\text{pl}} = 90^\circ$ . This difference in intensity profiles is reflected in the qualitatively different behavior of the sublevel populations. Indeed, it follows from symmetry considerations that the statistical tensor  $\mathcal{A}_{10}$  vanishes for an ‘‘atom + light’’ system with the quantization axis in the plane of symmetry [46]. This is the case for the pure Bessel beam (5) and the superposition (9) with  $\phi_{\text{pl}} = 0^\circ$  [see Figs. 3(a) and 3(b)]. In contrast, a system with broken symmetry with respect to the  $x$ - $z$  plane is characterized by  $\mathcal{A}_{10} \neq 0$ , implying  $\rho_{-1/2}(t) \neq \rho_{+1/2}(t)$  [see Eq. (22)]. This is the case for the superposition (9) with  $\phi_{\text{pl}} = 90^\circ$ , displayed in Fig. 3(c).

In addition to analysis of the beam-intensity profiles, another approach can be used to understand—at least qualitatively—the behavior of the magnetic sublevel

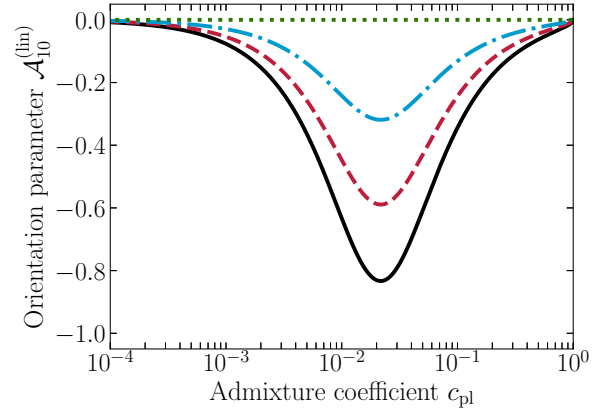


FIG. 4. Orientation parameter (25) of the  $5s^2S_{1/2}$  state of Rb as a function of the weight  $c_{\text{pl}}$  of the plane-wave component obtained from the perturbative analysis of photoexcitation and decay for  $B = 0$ . Calculations were performed for  $\phi_{\text{pl}} = 90^\circ$  (solid line),  $\phi_{\text{pl}} = 45^\circ$  (dashed line),  $\phi_{\text{pl}} = 22.5^\circ$  (dash-dotted line), and  $\phi_{\text{pl}} = 0^\circ$  (dotted line). All other parameters are the same as in Fig. 3.

populations  $\rho_{\pm 1/2}(t)$ . This approach is based on the perturbative analysis of the excitation and decay of a target atom interacting with incoming twisted light. It is very close to that used for description of the resonant elastic scattering discussed in detail in Refs. [48,49] and employs second-order perturbation theory. For brevity, we will not repeat the calculation steps here and just present the perturbative prediction for the orientation parameter of the  $5s^2S_{1/2}$  state:

$$\mathcal{A}_{10}^{(\text{lin})} = -\frac{10c_{\text{pl}}\sqrt{1 - c_{\text{pl}}^2}\sin(\theta_k)\sin(\phi_{\text{pl}})}{12c_{\text{pl}}^2 + 3(1 - c_{\text{pl}}^2)\sin^2(\theta_k)}. \quad (25)$$

This result is obtained for the vector potential (9) and hence depends on the weight  $c_{\text{pl}}$  and phase  $\phi_{\text{pl}}$  of the plane-wave component, as well as on the opening angle  $\theta_k$  of the Bessel beam. Figure 4 shows the predictions of Eq. (25) as a function of the weight  $c_{\text{pl}}$  for  $\theta_k = 2.49^\circ$  and different relative phases  $\phi_{\text{pl}}$ . As seen from Fig. 4, the orientation parameter  $\mathcal{A}_{10}^{(\text{lin})}$  vanishes in the limit of a pure plane wave,  $c_{\text{pl}} = 1$ , and a pure Bessel beam,  $c_{\text{pl}} = 0$ . This thus confirms the results of the time-dependent density-matrix calculations. Moreover, perturbation theory predicts a strong dependence of  $\mathcal{A}_{10}^{(\text{lin})}$  on the relative phase  $\phi_{\text{pl}}$  between the Bessel and plane-wave components. For example, when  $\phi_{\text{pl}} = 0^\circ$ , there is no orientation of the ground state, regardless of the weight  $c_{\text{pl}}$ . This agrees with the conclusion based on the analysis of intensity profiles. In addition, remarkable orientation of the ground state can be observed for  $\phi_{\text{pl}} \neq 0$  and weight coefficients  $0.001 \leq c_{\text{pl}} \leq 0.1$ . For instance, for  $\phi_{\text{pl}} = 90^\circ$  and  $c_{\text{pl}} = 0.1$  naive perturbation theory predicts  $\mathcal{A}_{10}^{(\text{lin})} = -0.34$ , in qualitative agreement with the result obtained by solving the Liouville–von Neumann equation,  $\mathcal{A}_{10}^{(\text{lin})} = -0.56$ . We also note from Eq. (25) that the peak position  $c_{\text{pl}}^{(\text{peak})}$  of the orientation parameter  $\mathcal{A}_{10}^{(\text{lin})}$  depends on the opening angle  $\theta_k$ :

$$c_{\text{pl}}^{(\text{peak})} = \frac{\sin(\theta_k)}{\sqrt{4 + \sin^2(\theta_k)}}. \quad (26)$$

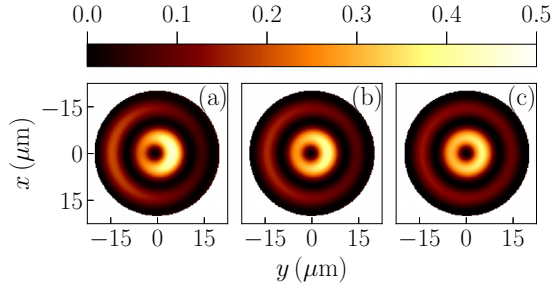


FIG. 5. Same as the right column of Fig. 3, but for  $\phi_{\text{pl}} = 90^\circ$  and (a)  $c_{\text{pl}} = 0.1$ , (b)  $c_{\text{pl}} = 0.06$ , and (c)  $c_{\text{pl}} = 0.03$ .

In particular, for  $\theta_k = 2.49^\circ$  the peak is located at  $c_{\text{pl}}^{\text{(peak)}} = 0.022$  (see Fig. 4).

Both Eq. (25), based on the perturbation theory approach, and the more accurate density-matrix predictions of Eqs. (17) show that the orientation parameter of the  $5s^2S_{1/2}$  ground state is very sensitive to the phase  $\phi_{\text{pl}}$  and the weight  $c_{\text{pl}}$  of the plane-wave component. This sensitivity is most pronounced for rather small weights in the range from 0.001 to 0.1. For such tiny parameters  $c_{\text{pl}}$ , it is very difficult to infer any composition of the incident beam (9) from the intensity profile. For example, the superpositions with  $c_{\text{pl}} = 0.1$ ,  $c_{\text{pl}} = 0.06$ , and  $c_{\text{pl}} = 0.03$  exhibit very similar intensity profiles, as displayed in Fig. 5, while the corresponding orientation parameters  $\mathcal{A}_{10}^{(\text{lin})} = -0.34$ ,  $\mathcal{A}_{10}^{(\text{lin})} = -0.53$ , and  $\mathcal{A}_{10}^{(\text{lin})} = -0.79$  are clearly distinguishable and relatively easy to observe in modern experiments.

### B. Magnetic-field dependence

In the previous section we showed that the orientation of the  $5s^2S_{1/2}$  ground state of the target atom is very sensitive to the weight and relative phase of the plane-wave admixture to the dominant twisted mode. We argue, therefore, that measurements of the atomic orientation can be used to study the beam composition. In order to make the proposed diagnostic method even more accessible, it is convenient to introduce one more physical parameter whose variation would affect  $\mathcal{A}_{10}$ . The applied magnetic-field strength  $B$  may be such a parameter. As we have already mentioned, the atomic quantization axis is chosen to be along  $\mathbf{B}$ , which is perpendicular to both the light propagation and polarization directions.

The magnetic-field dependence of the steady-state sublevel population of the  $5s^2S_{1/2}$  state, produced in the course of the interaction with the  $y$ -polarized Bessel-wave + plane-wave mixture, is shown in Fig. 6. Here, calculations were performed for fixed weight  $c_{\text{pl}} = 0.1$  but different phases  $\phi_{\text{pl}}$ . Moreover, the magnetic-field strength lies in the range  $0 \leq B \leq 0.5$  mT, so that the Zeeman splitting of the  $5p^2P_{3/2}$  level is comparable with the natural width of the transition. As seen from Fig. 6, the orientation parameter is very sensitive to  $B$ . In particular, the orientation of the ground state is most pronounced for small values of magnetic field and then decreases with  $B$ . For  $\phi_{\text{pl}} = 90^\circ$ , the orientation parameter takes the value  $\mathcal{A}_{10}^{(\text{lin})} \approx -0.56$  at  $B = 0$  but is reduced to  $\mathcal{A}_{10}^{(\text{lin})} \approx -0.11$  at  $B = 0.5$  mT. This behavior agrees with the predictions of perturbation theory. Indeed, a formula similar to Eq. (25) can be

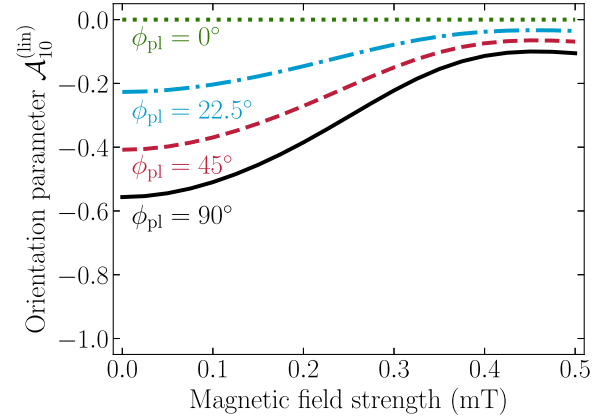


FIG. 6. Orientation parameter  $\mathcal{A}_{10}^{(\text{lin})}$  of the  $5s^2S_{1/2}$  state of Rb as a function of the magnetic-field strength for fixed weight  $c_{\text{pl}} = 0.1$  and different relative phases of the plane-wave component:  $\phi_{\text{pl}} = 90^\circ$  (solid line),  $\phi_{\text{pl}} = 45^\circ$  (dashed line),  $\phi_{\text{pl}} = 22.5^\circ$  (dash-dotted line), and  $\phi_{\text{pl}} = 0^\circ$  (dotted line). All other parameters are the same as in Fig. 3.

derived for a nonvanishing magnetic field, which shows that  $\mathcal{A}_{10}^{(\text{lin})}(B)$  is monotonically decreasing. This formula is rather complicated and for brevity will not be shown here.

While Fig. 6 shows  $\mathcal{A}_{10}^{(\text{lin})}(B)$  for different relative phases  $\phi_{\text{pl}}$ , Fig. 7 illustrates how the orientation of the  $5s^2S_{1/2}$  state varies with weight  $c_{\text{pl}}$ . In Fig. 7 we find an ordering of  $\mathcal{A}_{10}^{(\text{lin})}$  which might seem counterintuitive at first sight. Namely, while the atomic orientation vanishes in the limit of a pure Bessel beam,  $c_{\text{pl}} = 0$ , we obtain  $\mathcal{A}_{10}^{(\text{lin})} \approx 0.1$  for  $c_{\text{pl}} = 0.001$ . Then the parameter  $\mathcal{A}_{10}^{(\text{lin})}$  reaches a maximum absolute value when  $c_{\text{pl}} = 0.01$  and decreases again for  $c_{\text{pl}} = 0.1$ . This behavior is not surprising since it reflects the  $c_{\text{pl}}$  dependence of  $\mathcal{A}_{10}^{(\text{lin})}$  shown in Fig. 4. We also see from Fig. 7 that the sensitivity of the orientation parameter  $\mathcal{A}_{10}^{(\text{lin})}(B)$  depends on the weight  $c_{\text{pl}}$ . For example, while  $\mathcal{A}_{10}^{(\text{lin})}$  varies from  $-0.56$  to  $-0.11$  for  $c_{\text{pl}} = 0.1$ , it remains almost constant for  $c_{\text{pl}} =$

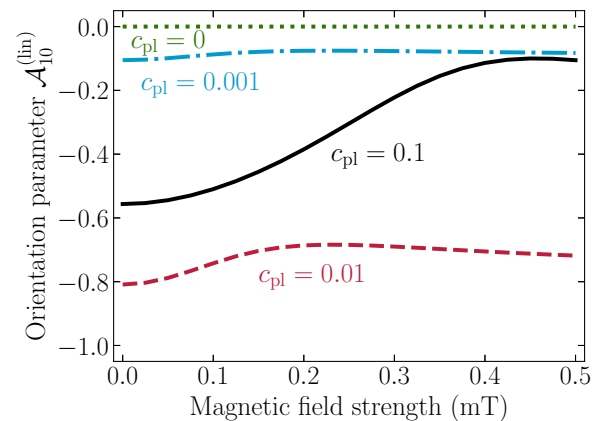


FIG. 7. Same as Fig. 6, but for fixed phase  $\phi_{\text{pl}} = 90^\circ$  and different weights of the plane-wave component:  $c_{\text{pl}} = 0.1$  (solid line),  $c_{\text{pl}} = 0.01$  (dashed line),  $c_{\text{pl}} = 0.001$  (dash-dotted line), and  $c_{\text{pl}} = 0$  (dotted line).

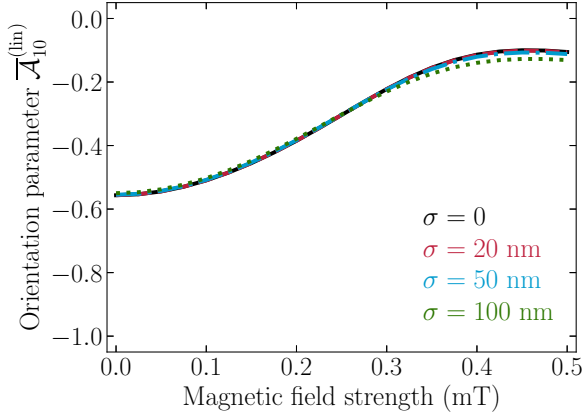


FIG. 8. Same as Fig. 6, but for fixed weight  $c_{\text{pl}} = 0.1$ , phase  $\phi_{\text{pl}} = 90^\circ$ , and different sizes of the atomic target:  $\sigma = 0$  (solid line),  $\sigma = 20$  nm (dashed line),  $\sigma = 50$  nm (dash-dotted line), and  $\sigma = 100$  nm (dotted line).

0.001. Such  $B$  dependence can naturally be used in experiments to analyze the weight of a plane-wave admixture.

### C. Delocalized atom

All calculations above were carried out for an atom perfectly localized in the beam center at  $b = 0$ . Such a perfect localization is, however, unrealistic experimentally since laser jittering and thermal distribution of trapped atoms cause uncertainty in the determination of the impact parameter  $\mathbf{b}$ . To take into account such delocalization, we assume that the probability to find an atom at a distance  $\mathbf{b}$  from the beam center is given by

$$f(\mathbf{b}) = \frac{1}{2\pi\sigma^2} e^{-\frac{b^2}{2\sigma^2}}, \quad (27)$$

with  $\sigma$  being the width [28,29]. By using  $f(\mathbf{b})$ , one can calculate the average sublevel population

$$\bar{\rho}_{M_g}(t) = \int f(\mathbf{b}) \rho_{M_g}(t) d^2\mathbf{b} \quad (28)$$

and the average orientation parameter  $\bar{\mathcal{A}}_{10} = [\bar{\rho}_{+1/2}(t) - \bar{\rho}_{-1/2}(t)] / [\bar{\rho}_{+1/2}(t) + \bar{\rho}_{-1/2}(t)]$ . In the past this semiclassical approach was successfully employed to describe the excitation of a trapped ion by twisted radiation [17].

The average effective orientation parameter  $\bar{\mathcal{A}}_{10}^{(\text{lin})}$  is displayed in Fig. 8 as a function of  $B$  for the mixture coefficient  $c_{\text{pl}} = 0.1$  and phase  $\phi_{\text{pl}} = 90^\circ$ . In order to illustrate the atom delocalization effect, calculations were performed for  $\sigma = 20$  nm,  $\sigma = 50$  nm, and  $\sigma = 100$  nm and compared with the idealized case of  $\sigma = 0$ . As seen from Fig. 8, the delocalization of the target atom has a minor effect on the orientation parameter  $\mathcal{A}_{10}^{(\text{lin})}$ . This indicates that the proposed method for diagnostics of twisted light beams can be realized under experimental conditions.

### D. Light polarization effects

So far we have considered the superposition (9) in which both the Bessel- and plane-wave components are linearly

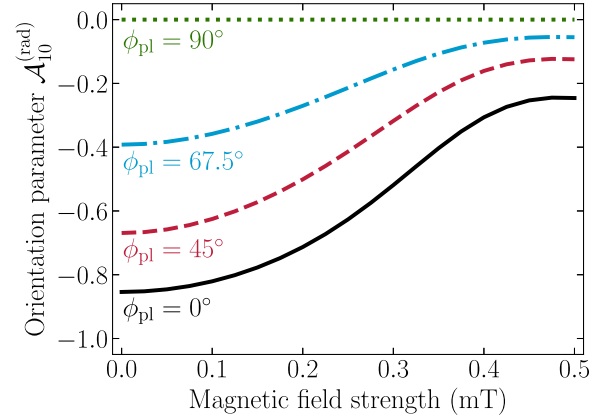


FIG. 9. Same as Fig. 6, but for the superposition (9) of the radially polarized Bessel beam and  $y$ -polarized plane wave. Results are shown for fixed weight  $c_{\text{pl}} = 0.1$  and different phases of the plane-wave component:  $\phi_{\text{pl}} = 0^\circ$  (solid line),  $\phi_{\text{pl}} = 45^\circ$  (dashed line),  $\phi_{\text{pl}} = 67.5^\circ$  (dash-dotted line), and  $\phi_{\text{pl}} = 90^\circ$  (dotted line).

polarized in the same direction. The theory developed in the present work, however, can be naturally extended to describe other polarization scenarios. For example, in the recent work of Lange *et al.* [17] the admixture of a linearly polarized plane wave to a radially polarized beam was suspected. In order to investigate this case, we performed detailed calculations of the orientation parameter  $\mathcal{A}_{10}^{(\text{rad})}$  of the  $5s^2S_{1/2}$  state for various values of the weight  $c_{\text{pl}}$  and phase  $\phi_{\text{pl}}$ . Like before, we found that  $\mathcal{A}_{10}^{(\text{rad})}$  vanishes for the cases of pure Bessel and plane waves but reaches significant values for their mixture. Figure 9 shows the magnetic-field dependence of  $\mathcal{A}_{10}^{(\text{rad})}$  calculated for  $c_{\text{pl}} = 0.1$  and several relative phases  $\phi_{\text{pl}}$ . As seen Fig. 9, the  $B$  dependence of  $\mathcal{A}_{10}^{(\text{rad})}$  qualitatively resembles what has been observed for the linearly polarized Bessel beam (see Fig. 6). The atomic orientation parameter  $\mathcal{A}_{10}^{(\text{rad})}$  shows the opposite dependence on  $\phi_{\text{pl}}$  compared to  $\mathcal{A}_{10}^{(\text{lin})}$ , as  $\mathcal{A}_{10}^{(\text{rad})}$  vanishes at  $\phi_{\text{pl}} = 90^\circ$  and reaches its maximum absolute values at  $\phi_{\text{pl}} = 0^\circ$ . For zero magnetic field,  $B = 0$ , this behavior is again confirmed by the expression

$$\mathcal{A}_{10}^{(\text{rad})} = -\frac{5c_{\text{pl}}\sqrt{1-c_{\text{pl}}^2}\sin(\theta_k)\cos(\phi_{\text{pl}})}{3c_{\text{pl}}^2+3(1-c_{\text{pl}}^2)\sin^2(\theta_k)}, \quad (29)$$

derived from second-order perturbation theory.

While Fig. 9 shows the  $\phi_{\text{pl}}$  dependence of the orientation parameter  $\mathcal{A}_{10}^{(\text{rad})}(B)$ , Fig. 10 displays the dependence on the weight  $c_{\text{pl}}$ . Like in the case of linear polarization, we observe that the variation of  $\mathcal{A}_{10}^{(\text{rad})}$  with magnetic-field strength is again very sensitive to the plane-wave admixture.

In contrast to linearly and radially polarized Bessel beams, the proposed method does not allow us to identify the admixture of a plane wave to an azimuthally polarized beam. Our theoretical analysis has shown that  $\mathcal{A}_{10}^{(\text{az})}$  vanishes for any combination of  $c_{\text{pl}}$  and  $\phi_{\text{pl}}$  if the atom is perfectly localized at  $b = 0$ . This is consistent with the analysis of the beam-intensity profiles and second-order perturbation calculations.



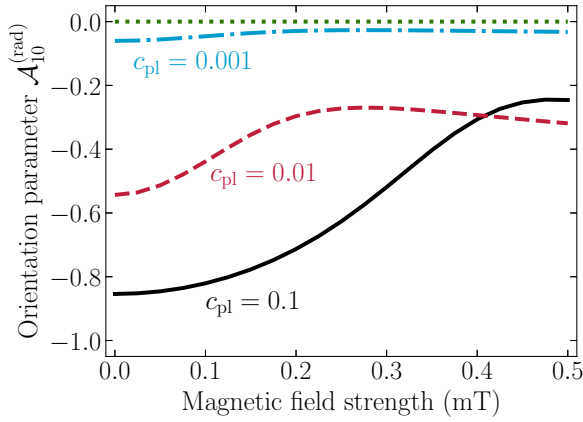


FIG. 10. Same as Fig. 7, but for the superposition (9) of the radially polarized Bessel beam and  $y$ -polarized plane wave. Calculations were performed for fixed phase  $\phi_{pl} = 0^\circ$  and different weights of the plane-wave component:  $c_{pl} = 0.1$  (solid line),  $c_{pl} = 0.01$  (dashed line),  $c_{pl} = 0.001$  (dash-dotted line), and  $c_{pl} = 0$  (dotted line).

However, this insensitivity is partially removed for the delocalized atom, as will be shown below.

Figure 11 shows the average orientation parameters  $\bar{A}_{10}$  for linearly, radially, and azimuthally polarized Bessel beams contaminated with a linearly polarized plane wave. Calculations were done for weight  $c_{pl} = 0.1$ , phase  $\phi_{pl} = 45^\circ$ , and target size  $\sigma = 50$  nm. As seen from Fig. 11,  $\bar{A}_{10}$  is very sensitive to both the polarization of light and the magnetic field. For the cases of linearly and radially polarized Bessel beams, the orientation parameter lies in the range  $-0.41 \leq \bar{A}_{10}^{(lin)} \leq -0.07$  and  $-0.66 \leq \bar{A}_{10}^{(rad)} \leq -0.15$ , respectively, while for the azimuthally polarized beam  $\bar{A}_{10}^{(az)}$  changes slightly from 0 to  $-0.02$  as  $B$  increases.

In the present work, we have mainly focused on the scenario where the plane-wave contamination is linearly

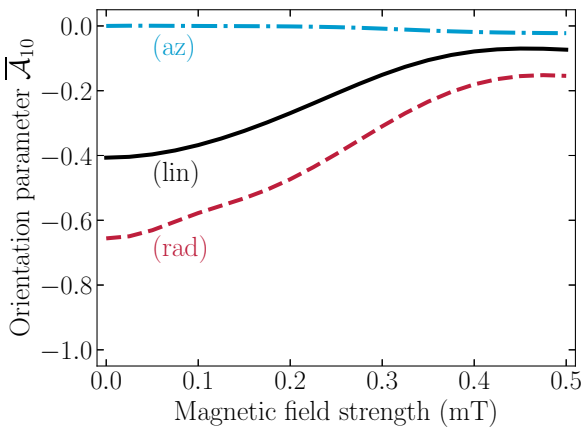


FIG. 11. Same as Fig. 6, but for fixed target size  $\sigma = 50$  nm and different compositions of radiation with  $c_{pl} = 0.1$  and  $\phi_{pl} = 45^\circ$ : linearly  $y$ -polarized Bessel wave + linearly  $y$ -polarized plane wave (solid line), radially polarized Bessel wave + linearly  $y$ -polarized plane wave (dashed line), and azimuthally polarized Bessel wave + linearly  $y$ -polarized plane wave (dash-dotted line).

polarized along the  $y$  axis. This choice was motivated by the conditions of a recent experiment performed by Lange *et al.* [17]. As mentioned above, however, our theoretical approach is general and can be used for any admixture mode. For the sake of brevity, we will not discuss the results in detail here and just mention two important findings. Namely, in the case of  $y$ -polarized Bessel and  $x$ -polarized plane waves, no atomic orientation occurs for any weight and phase of the mixture. In contrast, when the linearly polarized Bessel mode is contaminated by a circularly polarized plane wave, the atomic orientation vanishes at  $\phi_{pl} = 90^\circ$  and reaches its maximum absolute values at  $\phi_{pl} = 0^\circ$ . Again, both results agree with the intensity profile analysis and second-order perturbation calculations.

#### IV. SUMMARY AND OUTLOOK

In summary, we performed a theoretical analysis of the excitation of a single target atom by the superposition of twisted and plane waves. Special attention was paid to the magnetic sublevel population of the atomic ground state and to the question of how this population is affected by the weight and relative phase of the plane-wave admixture. In order to explore this sensitivity, we used a time-dependent density-matrix method based on the Liouville–von Neumann equation, from which we obtained the steady-state solution.

While the formalism developed here can be applied to any atom, in the present study we considered the  $5s \ ^2S_{1/2} - 5p \ ^2P_{3/2} E1$  transition in Rb induced by a superposition of twisted and plane waves. Based on the results of a recent trapped-ion experiment [17], we assumed that the plane-wave component is linearly polarized, while the twisted component can be linearly, radially, or azimuthally polarized. Detailed calculations demonstrated that the plane-wave admixture to twisted light can lead to significant orientation of the  $5s \ ^2S_{1/2}$  ground state, which is controlled by the external magnetic field. Furthermore, it was argued that the predicted high sensitivity of the target orientation holds under experimental conditions in which the atom is imprecisely localized with respect to the beam center.

Following our theoretical results, we propose that analysis of the atomic ground-state orientation can serve as a valuable tool for diagnostics of contaminated twisted light. It was demonstrated that the proposed method can be effective for detecting small admixtures, thus complementing traditional diagnostic approaches based on intensity profile analysis. An experiment to test this method is currently under development.

#### ACKNOWLEDGMENTS

This work was funded by the Deutsche Forschungsgemeinschaft (DFG, German Research Foundation) under Project ID No. 445408588 (SU 658/5-1) and Project ID No. 274200144, under SFB 1227 within Project No. B02 and under Germany's Excellence Strategy, EXC-2123 QuantumFrontiers, Project No. 390837967.

- [1] M. Padgett, Light's twist, *Proc. R. Soc. A* **470**, 20140633 (2014).
- [2] K. Y. Bliokh and F. Nori, Transverse and longitudinal angular momenta of light, *Phys. Rep.* **592**, 1 (2015).
- [3] H. Rubinsztein-Dunlop *et al.*, Roadmap on structured light, *J. Opt.* **19**, 013001 (2017).
- [4] G. Li, S. Zhang, L. Isenhower, K. Maller, and M. Saffman, Crossed vortex bottle beam trap for single-atom qubits, *Opt. Lett.* **37**, 851 (2012).
- [5] S. A. Kennedy, G. W. Biedermann, J. T. Farrar, T. G. Akin, S. P. Krzyzewski, and E. R. I. Abraham, Confinement of ultracold atoms in a Laguerre-Gaussian laser beam created with diffractive optics, *Opt. Commun.* **321**, 110 (2014).
- [6] M. E. J. Friese, J. Enger, H. Rubinsztein-Dunlop, and N. R. Heckenberg, Optical angular-momentum transfer to trapped absorbing particles, *Phys. Rev. A* **54**, 1593 (1996).
- [7] M. Padgett and R. Bowman, Tweezers with a twist, *Nat. Photonics* **5**, 343 (2011).
- [8] M. Mirhosseini, O. S. Magaña-Loaiza, M. N. O'Sullivan, B. Rodenburg, M. Malik, M. P. J. Lavery, M. J. Padgett, D. J. Gauthier, and R. W. Boyd, High-dimensional quantum cryptography with twisted light, *New J. Phys.* **17**, 033033 (2015).
- [9] B. Ndagano, I. Nape, M. A. Cox, C. Rosales-Guzman, and A. Forbes, Creation and detection of vector vortex modes for classical and quantum communication, *J. Lightwave Technol.* **36**, 292 (2018).
- [10] M. Drechsler, S. Wolf, C. T. Schmiegelow, and F. Schmidt-Kaler, Optical superresolution sensing of a trapped ion's wave packet size, *Phys. Rev. Lett.* **127**, 143602 (2021).
- [11] J. Zeng, Y. Dong, J. Zhang, and J. Wang, The trend of structured light-induced force microscopy: A review, *J. Opt.* **25**, 023001 (2023).
- [12] S. Fühapter, A. Jesacher, S. Bernet, and M. Ritsch-Marte, Spiral phase contrast imaging in microscopy, *Opt. Express* **13**, 689 (2005).
- [13] J. Wang, W. Zhang, Q. Qi, S. Zheng, and L. Chen, Gradual edge enhancement in spiral phase contrast imaging with fractional vortex filters, *Sci. Rep.* **5**, 15826 (2015).
- [14] S. Qiu, J. Wang, F. Castellucci, M. Cao, S. Zhang, T. W. Clark, S. Franke-Arnold, H. Gao, and F. Li, Visualization of magnetic fields with cylindrical vector beams in a warm atomic vapor, *Photonics Res.* **9**, 2325 (2021).
- [15] F. Castellucci, T. W. Clark, A. Selyem, J. Wang, and S. Franke-Arnold, Atomic compass: Detecting 3D magnetic field alignment with vector vortex light, *Phys. Rev. Lett.* **127**, 233202 (2021).
- [16] C. T. Schmiegelow, J. Schulz, H. Kaufmann, T. Ruster, U. G. Poschinger, and F. Schmidt-Kaler, Transfer of optical orbital angular momentum to a bound electron, *Nat. Commun.* **7**, 12998 (2016).
- [17] R. Lange, N. Huntemann, A. A. Peshkov, A. Surzhykov, and E. Peik, Excitation of an electric octupole transition by twisted light, *Phys. Rev. Lett.* **129**, 253901 (2022).
- [18] A. Afanasev, C. E. Carlson, C. T. Schmiegelow, J. Schulz, F. Schmidt-Kaler, and M. Solyanik, Experimental verification of position-dependent angular-momentum selection rules for absorption of twisted light by a bound electron, *New J. Phys.* **20**, 023032 (2018).
- [19] R. Blatt and P. Zoller, Quantum jumps in atomic systems, *Eur. J. Phys.* **9**, 250 (1988).
- [20] A. A. Peshkov, E. Jordan, M. Kromrey, K. K. Mehta, T. E. Mehlstäubler, and A. Surzhykov, Excitation of forbidden electronic transitions in atoms by Hermite-Gaussian modes, *Ann. Phys. (Berlin, Ger.)* **535**, 2300204 (2023).
- [21] B. S. Davis, L. Kaplan, and J. H. McGuire, On the exchange of orbital angular momentum between twisted photons and atomic electrons, *J. Opt.* **15**, 035403 (2013).
- [22] S. M. Barnett and M. V. Berry, Superweak momentum transfer near optical vortices, *J. Opt.* **15**, 125701 (2013).
- [23] J. D. Rodrigues, L. G. Marcassa, and J. T. Mendonça, Excitation of high orbital angular momentum Rydberg states with Laguerre-Gauss beams, *J. Phys. B* **49**, 074007 (2016).
- [24] A. M. Akulshin, I. Novikova, E. E. Mikhailov, S. A. Suslov, and R. J. McLean, Arithmetic with optical topological charges in stepwise-excited Rb vapor, *Opt. Lett.* **41**, 1146 (2016).
- [25] G. F. Quinteiro, F. Schmidt-Kaler, and C. T. Schmiegelow, Twisted-light-ion interaction: The role of longitudinal fields, *Phys. Rev. Lett.* **119**, 253203 (2017).
- [26] M. Babiker, D. L. Andrews, and V. E. Lembessis, Atoms in complex twisted light, *J. Opt.* **21**, 013001 (2019).
- [27] G. De Ninno *et al.*, Photoelectric effect with a twist, *Nat. Photonics* **14**, 554 (2020).
- [28] B. A. Knyazev and V. G. Serbo, Beams of photons with nonzero projections of orbital angular momenta: New results, *Phys. Usp.* **61**, 449 (2018).
- [29] S. A.-L. Schulz, A. A. Peshkov, R. A. Müller, R. Lange, N. Huntemann, C. Tamm, E. Peik, and A. Surzhykov, Generalized excitation of atomic multipole transitions by twisted light modes, *Phys. Rev. A* **102**, 012812 (2020).
- [30] M. E. Rose, *Elementary Theory of Angular Momentum* (Wiley, New York, 1957).
- [31] C. Rosales-Guzmán, B. Ndagano, and A. Forbes, A review of complex vector light fields and their applications, *J. Opt.* **20**, 123001 (2018).
- [32] A. Lurio and R. Novick, Lifetime and hfs of the  $(5s5p)^1P_1$  state of cadmium, *Phys. Rev.* **134**, A608 (1964).
- [33] J. C. Lehmann and C. Cohen-Tannoudji, Pompage optique en champ magnétique faible, *C. R. Acad. Sci.* **258**, 4463 (1964).
- [34] L. R. Hunter, G. M. Watson, D. S. Weiss, and A. G. Zajonc, High-precision measurement of lifetimes and collisional decay parameters in Ca  $^1D$  states using the two-photon Hanle effect, *Phys. Rev. A* **31**, 2268 (1985).
- [35] E. Peik, G. Hollemann, C. A. Schrama, and H. Walther, Spectroscopy of a single trapped indium ion, *Laser Phys.* **4**, 376 (1994).
- [36] E. Breschi and A. Weis, Ground-state Hanle effect based on atomic alignment, *Phys. Rev. A* **86**, 053427 (2012).
- [37] W. R. Johnson, *Atomic Structure Theory* (Springer, New York, 2007).
- [38] A. Surzhykov, D. Seipt, V. G. Serbo, and S. Fritzsche, Interaction of twisted light with many-electron atoms and ions, *Phys. Rev. A* **91**, 013403 (2015).
- [39] M. Auzinsh, D. Budker, and S. M. Rochester, *Optically Polarized Atoms: Understanding Light-Atom Interactions* (Oxford University Press, Oxford, 2010).
- [40] J. P. Barrat and C. Cohen-Tannoudji, Étude du pompage optique dans le formalisme de la matrice densité, *J. Phys. Radium* **22**, 329 (1961).
- [41] P. Tremblay and C. Jacques, Optical pumping with two finite linewidth lasers, *Phys. Rev. A* **41**, 4989 (1990).

- [42] K. Blum, *Density Matrix Theory and Applications* (Springer, Berlin, 2012).
- [43] L. von der Wense, P. V. Bilous, B. Seiferle, S. Stellmer, J. Weitenberg, P. G. Thirolf, A. Pálffy, and G. Kazakov, The theory of direct laser excitation of nuclear transitions, *Eur. Phys. J. A* **56**, 176 (2020).
- [44] S. Stenholm, *Foundations of Laser Spectroscopy* (Wiley, New York, 1984).
- [45] F. Renzoni, W. Maichen, L. Windholz, and E. Arimondo, Coherent population trapping with losses observed on the Hanle effect of the  $D_1$  sodium line, *Phys. Rev. A* **55**, 3710 (1997).
- [46] V. V. Balashov, A. N. Grum-Grzhimailo, and N. M. Kabachnik, in *Polarization and Correlation Phenomena in Atomic Collisions: A Practical Theory Course*, edited by P. G. Burke and H. Kleinpoppen (Springer, Berlin, 2000).
- [47] S. Fritzsche, A fresh computational approach to atomic structures, processes and cascades, *Comput. Phys. Commun.* **240**, 1 (2019).
- [48] S. Roy, L. Kissel, and R. H. Pratt, Elastic scattering of photons, *Radiat. Phys. Chem.* **56**, 3 (1999).
- [49] V. G. Serbo, A. Surzhykov, and A. Volotka, Resonant scattering of plane-wave and twisted photons at the gamma factory, *Ann. Phys. (Berlin)* **534**, 2100199 (2022).